

Stacked Auto-encoders for Classification of 3D Spine Models in Adolescent Idiopathic Scoliosis

William E. Thong, Hubert Labelle, Jesse Shen, Stefan Parent
and Samuel Kadoury

Abstract Current classification systems for adolescent idiopathic scoliosis lack information on how the spine is deformed in three dimensions (3D), which can mislead further treatment recommendations. We propose an approach to address this issue by a deep learning method for the classification of 3D spine reconstructions of patients. A low-dimensional manifold representation of the spine models was learnt by stacked auto-encoders. A K-Means++ algorithm using a probabilistic seeding method clustered the low-dimensional codes to discover sub-groups in the studied population. We evaluated the method with a case series analysis of 155 patients with Lenke Type-1 thoracic spinal deformations recruited at our institution. The clustering algorithm proposed 5 sub-groups from the thoracic population, yielding statistically significant differences in clinical geometric indices between all clusters. These results demonstrate the presence of 3D variability within a pre-defined 2D group of spinal deformities.

Supported by the CHU Sainte-Justine Academic Research Chair in Spinal Deformities, the Canada Research Chair in Medical Imaging and Assisted Interventions, the 3D committee of the Scoliosis Research Society, the Natural Sciences and Engineering Research Council of Canada and the MEDITIS program.

W.E. Thong

MEDICAL, École Polytechnique de Montréal, Montréal, Canada
e-mail: william.thong@polymtl.ca

H. Labelle · J. Shen · S. Parent

Department of Surgery, CHU Sainte-Justine Research Center,
Université de Montréal, Montréal, Canada
e-mail: hubert.labelle@umontreal.ca

J. Shen

e-mail: jesse.shen@umontreal.ca

S. Parent

e-mail: stefan.parent@umontreal.ca

S. Kadoury (✉)

CHU Sainte-Justine Research Center, MEDICAL,
École Polytechnique de Montréal, Montréal, Canada
e-mail: samuel.kadoury@polymtl.ca

© Springer International Publishing Switzerland 2015

J. Yao et al. (eds.), *Recent Advances in Computational Methods and Clinical Applications for Spine Imaging*, Lecture Notes in Computational Vision and Biomechanics 20, DOI 10.1007/978-3-319-14148-0_2

1 Introduction

Adolescent idiopathic scoliosis (AIS) refers to a complex deformation in three dimensions (3D) of the spine. Classification of the rich and complex variability of spinal deformities is critical for comparisons between treatments and for long-term patient follow-ups. AIS characterization and treatment recommendations currently rely on the Lenke classification system [10] because of its simplicity and its high inter- and intra-observer reliability compared with previous classification systems [8]. However, these schemes are restricted to a two-dimensional (2D) assessment of scoliosis from radiographs of the spine in the coronal and sagittal planes. Misinterpretations could arise because two different scoliosis deformities may have similar 2D parameters. Therefore, improvements in the scoliosis classification system are necessary to ensure a better understanding and description of the curve morphology.

Computational methods open up new paths to go beyond the Lenke classification. Recent studies seek new groups in the population of AIS using cluster analysis [4, 5, 15, 17] with ISOData, K-Means or fuzzy C-Means algorithms. Their common aspect is founded upon the clustering of expert-based features, which are extracted from 3D spine reconstructions (Cobb angles, kyphosis and planes of maximal deformity). This methodology stems from the fact that clustering algorithms are very sensitive to the curse of dimensionality. Still, these parameters might not be enough to tap all the rich and complex variability in the data. Computational methods should be able to capture the intrinsic dimensionality that explains as much as possible the highly dimensional data into a manifold of much lower dimensionality [2, 11]. Hence, another paradigm for spine classification is to let the algorithm learn its own features to discriminate between different pathological groups. This implies directly analyzing the 3D spine models instead of expert-based features as it has been experimented previously. To our knowledge, only one study tried to learn a manifold from the 3D spine model [7] using Local Linear Embeddings (LLE). In this study, we propose to use stacked auto-encoders—a deep learning algorithm—to reduce the high-dimensionality of 3D spine models in order to identify particular classes within Lenke Type-1 curves. This algorithm was able to outperform principal component analysis (PCA) and LLE [6, 11].

Recent breakthroughs in computer vision and speech processing using deep learning algorithms suggest that artificial neural networks might be better suited to learn representations of highly non-linear data [2]. Training a deep neural network has been a challenging task in many applications. Nowadays, this issue is tackled by leveraging more computation power (i.e. parallelizing tasks), more data and by a better initialization of the multilayer neural network [6]. Deep neural networks promote the learning of more abstract representations that result in improved generalization. Network depth actually helps to become invariant to most local changes in the data and to disentangle the main factor of variations in the data [2].

We propose a computational method for the classification of highly dimensional 3D spine models obtained from a group of patients with AIS. The core of the methodology, detailed in Sect. 2, builds a low-dimensional representation of the 3D

spine model based on stacked auto-encoders that capture the main variabilities in the shape of the spine. The low-dimensional codes learnt by the stacked auto-encoders are then clustered using the K-Means++ algorithm. Finally, a statistical analysis assesses the relevance of the clusters identified by the framework based on clinical geometrical indices of the spine. Experiments conducted with this methodology are shown and discussed in Sect. 3, while Sect. 4 concludes this paper.

2 Methods

The proposed method consists of four main steps: (1) reconstruction of a 3D spine model from biplanar X-rays for each patient; (2) dimensionality reduction of each high-dimensional model to a low-dimensional space; (3) clustering of the low-dimensional space; (4) analysis of the clusters obtained with the clinical data.

2.1 3D Spine Reconstruction

A 3D model for each patient's spine was generated from anatomical landmarks with a semi-supervised statistical image-based technique built in a custom software in C++ [13]. Seventeen 3D anatomical landmarks were extracted per vertebra (12 thoracic, 5 lumbar): center, left, right, anterior and posterior of superior and inferior vertebral endplates (10 landmarks); left and right transverse process (2 landmarks); spinous process (1 landmark); and tips of both pedicles (4 landmarks). All 3D spine models were normalized with regards to their height and rigidly translated to a common referential at the L5 vertebra. Hence, each observation contains 867 features, which corresponds to the concatenation of the 3D coordinates of all the landmarks into an observation vector.

2.2 Stacked Auto-encoders for Dimensionality Reduction

An auto-encoder is a neural network that learns a hidden representation to reconstruct its input. Consider a one hidden layer auto-encoder network. First, the input vector \mathbf{x} of dimension d , representing the 3D coordinates of a spine model, is mapped by an encoder function f into the hidden layer \mathbf{h} , often called a code layer in the case of auto-encoders:

$$\mathbf{h} = f(\mathbf{x}) = s(-\mathbf{W}^{(1)}\mathbf{x} + \mathbf{b}^{(1)}) \quad (1)$$

where $\mathbf{W}^{(1)}$ is the encoding weight matrix, $\mathbf{b}^{(1)}$ the bias vector and $s(\cdot)$ the activation function. Note that this one hidden layer auto-encoder network corresponds to a principal component analysis if the activation function is linear. Then, the code

representation is mapped back by a decoder function g into a reconstruction \mathbf{z} :

$$\mathbf{z} = g(f(\mathbf{x})) = s(-\mathbf{W}^{(2)}\mathbf{h} + \mathbf{b}^{(2)}) \quad (2)$$

where $\mathbf{W}^{(2)}$ is the decoding weight matrix. Tying the weights ($\mathbf{W}^{(2)} = \mathbf{W}^{(1)T}$) has several advantages. It acts as a regularizer by preventing tiny gradients and it reduces the number of parameters to optimize [2]. Finally, the parameters $\theta = \{\mathbf{W}^{(1)}, \mathbf{b}^{(1)}, \mathbf{b}^{(2)}\}$ are optimized in order to minimize the squared reconstruction error:

$$L_2(\mathbf{x}, \mathbf{z}) = \|\mathbf{x} - \mathbf{z}\|^2. \quad (3)$$

In the case of dimensionality reduction, the code layer \mathbf{h} has a smaller dimension than the input \mathbf{x} . One major drawback comes from the gradient descent algorithm for the training procedure that is very sensitive to the initial weights. If they are far from a good solution, training a deep non-linear auto-encoder network is very hard [6]. A pre-training algorithm is thus required to learn more robust features before fine-tuning the whole model.

The idea for initialization is to build a model that reconstructs the input based on a corrupted version of itself. This can either be done by Restricted Boltzmann Machines (RBMs) [6] or denoising auto-encoders [18] (used in this study). The denoising auto-encoder is considered as a stochastic version of the auto-encoder [18]. The difference lies in the stochastic corruption process that sets randomly some of the inputs to zero. This corrupted version $\tilde{\mathbf{x}}$ of the input \mathbf{x} is obtained by a stochastic mapping $\tilde{\mathbf{x}} \sim q_D(\tilde{\mathbf{x}}|\mathbf{x})$ with a proportion of corruption v . The denoising auto-encoder is then trained to reconstruct the uncorrupted version of the input from the corrupted version, which means that the loss function in Eq. 3 remains the same. Therefore, the learning process tries to cancel the stochastic corruption process by capturing the statistical dependencies between the inputs [2]. Once all the layers are pre-trained, the auto-encoder proceeds to a fine-tuning of the parameters θ (i.e. without the corruption process).

2.3 *K-Means++ Clustering Algorithm*

Once the fine-tuning of the stacked auto-encoder has learnt the parameters θ , low-dimensional codes from the code layer can be extracted for each patient's spine. Clusters in the codes were obtained using the K-Means++ algorithm [1], which is a variant of the traditional K-Means clustering algorithm but with a selective seeding process. First, a cluster centroid is initialized among a random code layer \mathbf{h} of the dataset χ following a uniform distribution. Afterwards, a probability is assigned to the rest of the observations for choosing the next centroid:

$$p(\mathbf{h}) = \frac{D(\mathbf{h})^2}{\sum_{h \in \chi} D(\mathbf{h})^2} \quad (4)$$

where $D(\mathbf{h})^2$ corresponds to the shortest distance from a point \mathbf{h} to its closest cluster centroid. After the initialization of the cluster centroids, the K-Means++ algorithm proceeds to the regular Lloyd's optimization method.

The selection of the right number of clusters k is based on the validity ratio [14], which minimizes the intra-cluster distance and maximizes the inter-cluster distance. The ratio is defined as $validity = intra/inter$. The intra-cluster distance is the average of all the distances between a point and its cluster centroid:

$$intra = \frac{1}{N} \sum_{i=1}^k \sum_{\mathbf{x} \in C_i} \|\mathbf{h} - \mathbf{c}_i\|^2. \quad (5)$$

where N is the number of observations in χ and \mathbf{c}_i the centroid of cluster i . The inter-cluster distance is the minimum distance between cluster centroids.

$$inter = \min(\|\mathbf{c}_i - \mathbf{c}_j\|^2) \quad (6)$$

where $i = 1, 2, \dots, k-1$ and $j = i+1, \dots, k$.

2.4 Clinical Data Analysis

Once clusters were created from the low-dimensional representation of the dataset, we analyzed the clustered data points with 3D geometric indices in the main thoracic (MT) and thoracolumbar/lumbar (TLL) regions for each patient's spine. One-way ANOVA tested differences between the cluster groups with a significance level $\alpha = 0.05$. The p -values were adjusted with the Bonferroni correction. For all cases, the following 3D spinal indices were computed: the orientation of the plane of maximum curvature (PMC) in each regional curve, which corresponds to the plane orientation where the projected Cobb angle is maximal; the kyphotic angle, measured between T2 and T12 on the sagittal plane; the lumbar lordosis angle, defined between L1 and S1 on the sagittal plane; the Cobb angles in the MT and TLL segments; and the axial orientation of the apical vertebra in the MT region, measured by the Stokes method [16].

3 Clinical Experiments

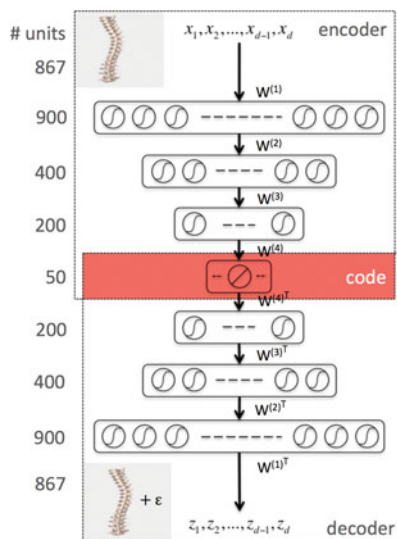
3.1 Clinical Data

A cohort of 155 AIS patients was recruited for this preliminary study at our institution. A total of 277 reconstructions of the spine was obtained in 3D. From this group, 60 patients had repeat measurements from multiple clinic visits (mean = 3 visits). The mean thoracic Cobb angle was $53.2 \pm 18.3^\circ$ (range = 11.2 – 100.2°). All patients were diagnosed with a right thoracic deformation and classified as Lenke Type-1 deformity. A lumbar spine modifier (A, B, C) was also assigned to each observation, using the biplanar X-Ray scans available for each patient. The dataset included 277 observations divided in 204 Lenke Type-1A, 43 Lenke Type-1B and 30 Lenke Type-1C deformities. The training set included 235 observations, while the validation set included 42 observations (15 % of the whole dataset). Observations were randomly assigned in each set.

3.2 Hyper-Parameters of the Stacked Auto-Encoders

The neural network hyper-parameters were chosen by an exhaustive grid search. The architecture yielding to the lowest validation mean squared error (MSE) is described in Fig. 1. We used an encoder with layers of size 867-900-400-200-50 and a decoder with tied weights to map the high-dimensional patient's spine models into low-

Fig. 1 Illustration of the stacked auto-encoders architecture to learn the 3D spine model by minimizing the loss function. The middle layer represents a low-dimensional representation of the data, called the code layer. An optimal layer architecture of 867-900-400-200-50 was found after a coarse grid search of the hyper-parameters



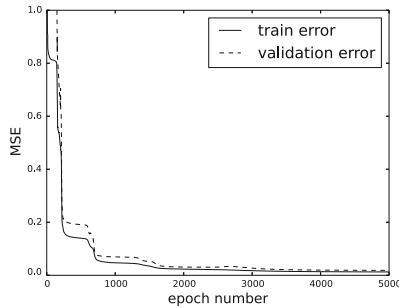


Fig. 2 Evolution of the mean squared error (MSE) with respect to the number of epochs to determine the optimal model described in Fig. 1

dimensional codes. All units in the network were activated by a sigmoidal function $s(a) = 1/(1 + e^{-a})$, except for the 50 units in the code layer that remain linear $s(a) = a$.

3.3 Training and Testing the Stacked Auto-encoders

Auto-encoder layers were pre-trained and fine-tuned with the stochastic gradient descent method using a GPU implementation based on the Theano library [3]. Pre-training had a proportion of corruption for the stochastic mapping in each hidden layer of $v = \{0.15, 0.20, 0.25, 0.30\}$ and a learning rate of $\varepsilon_0 = 0.01$. Fine-tuning ran for 5,000 epochs and had a learning rate schedule with $\varepsilon_0 = 0.05$ that annihilates linearly after 1,000 epochs. Figure 2 shows the learning curve of the stacked auto-encoder. The optimal parameters θ for the model in Fig. 1 were found at the end of training with a normalized training MSE of 0.0127, and a normalized validation MSE of 0.0186, which corresponds to 4.79 and 6.46 mm² respectively on the original scale. The learning curve describes several flat regions before stabilizing after 3,500 epochs.

3.4 Clustering the Codes

The K-Means++ algorithm was done using the scikit-learn library [12]. For each number of clusters k (2 through 9), the algorithm ran for 100 times with different centroid seeds in order to keep the best clustering in terms of inertia. Figure 3 depicts the validity ratio against the number of clusters. The validity ratio suggests that the optimal number of clusters should be 4 or 5. However, subsequent analysis illustrated in Table 1 indicates that 5 clusters is the right number of clusters for this dataset because all the clinical indices are statistically significant ($\alpha = 0.05$) given that the other indices are in the model. Figure 4 presents the visualization of the five

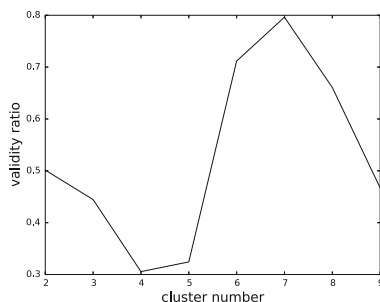


Fig. 3 Validity ratio with respect to the number of clusters, to determine the optimal number of clusters

clusters using a PCA to project the codes in 3D and 2D views. However, it should be mentioned that the clustering was performed on the codes of dimension 50. Figure 5 shows the frontal, lateral and daVinci representations of the centroid of each cluster.

3.5 Clinical Significance

Based on the five identified clusters, cluster 1 is composed of 50 Lenke Type-1A, 12 Type-1B and 2 Type-1C, representing hyper-kyphotic, hyper-lordotic profiles, with high curvatures in the sagittal plane. No sagittal rotation was detected in cluster 1. Cluster 2 is composed of 29 Lenke Type-1A, 7 Type-1B and 0 Type-1C, representing a high axial rotation of the apical vertebra, with the strongest thoracic deformation of all clusters. Moreover, those two clusters have no lumbar derotation.

Clusters 3, 4 and 5 represent the clusters with higher lumbar deformities. Cluster 3 includes 34 Lenke Type-1A, 17 Type-1B and 20 Type-1C, with a minimal thoracic deformation and the highest angulation of TLL plane of all clusters. Cluster 4 includes 23 observations, with 21 Lenke Type-1A, 2 Type-1B and 0 Type-1C. Cluster 4 is characterized by a hypo-kyphotic profile (mean = 7°) and the highest angulation of the MT plane of all clusters. Finally, cluster 5 includes 70 Lenke Type-1A, 5 Type-1B and 8 Type-1C, with a low kyphosis, and medium range thoracic deformations. While this last cluster has a higher orientation of the thoracolumbar curve, its magnitude is not significant.

Surgical strategies based on current 2D classification systems are suboptimal since they do not capture the intrinsic 3D representation of the deformation. Lenke Type-1 classification currently leads to selective thoracic arthrodesis. This very restrictive surgery treatment comes from the hard thresholds on the geometric parameters. A small change in Cobb angle could lead to two different classifications and to two different fusion recommendations subsequently [9]. Therefore, identifying groups based on their true 3D representation will help to better adjust surgery choices such as levels of fusion, biomechanical forces to apply or surgical instrumentations.

Table 1 Mean geometric clinical 3D parameters for the thoracic and lumbar regions, within all five clusters detected by the framework

Parameter (all in degrees)	Cluster 1 (n = 64)	Cluster 2 (n = 36)	Cluster 3 (n = 71)	Cluster 4 (n = 23)	Cluster 5 (n = 83)	p-value _{adj}
PMC MT Cobb	50.6 ± 13.8	73.3 ± 12.7	43.3 ± 15.5	62.2 ± 9.2	52.5 ± 14.6	<0.001*
PMC MT Orient	71.6 ± 12.1	78.1 ± 7.5	72.5 ± 12.1	88.5 ± 4.1	82.0 ± 10.4	<0.001*
PMC TLL Cobb	34.1 ± 12.7	49.5 ± 11.6	36.2 ± 15.1	38.2 ± 12.1	36.6 ± 13.3	<0.001*
PMC TLL Orient	45.4 ± 18.9	51.3 ± 15.0	65.0 ± 24.0	52.8 ± 12.2	48.4 ± 17.3	<0.001*
Kyphosis	36.6 ± 10.6	32.4 ± 11.2	27.4 ± 9.8	7.3 ± 11.6	21.9 ± 11.7	<0.001*
Lordosis	-66.6 ± 8.9	-63.4 ± 14.1	-61.6 ± 12.3	-54.2 ± 13.1	-60.9 ± 9.7	0.002*
MT Cobb	46.6 ± 22.2	69.2 ± 24.8	43.3 ± 15.6	62.2 ± 9.2	50.9 ± 18.4	<0.001*
TLL Cobb	-29.9 ± 22.2	-45.5 ± 25.5	-36.3 ± 14.9	-38.2 ± 12.1	-34.8 ± 18.3	0.036*
Ax. rot. apex	-19.7 ± 10.3	-33.8 ± 7.6	-13.7 ± 8.7	-25.9 ± 8.8	-22.1 ± 12.0	<0.001*

A significant star (*) indicates that the differences of geometric parameter between all groups are statistically significant at level $\alpha = 0.05$, given that the other geometric parameters are in the model

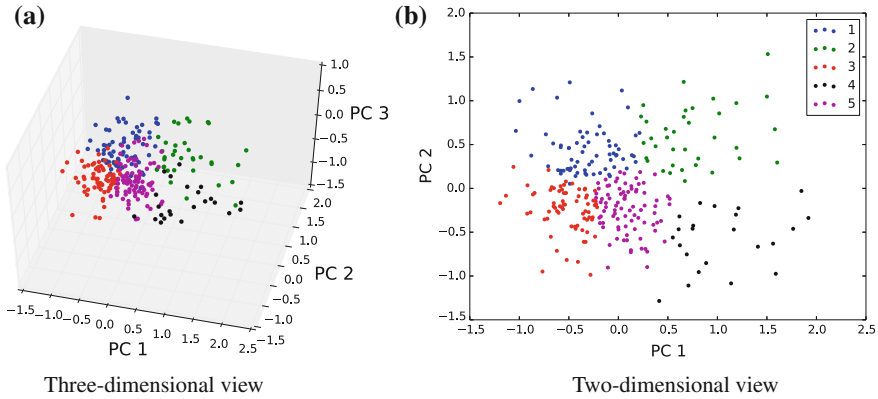


Fig. 4 Visualization of the five clusters found by the K-Means++ algorithm on low-dimensional points, by projecting the 50-dimensional codes into 3 (a) and 2 (b) principal components (PC) using PCA

In this study, the learning framework provided an optimal number of 5 clusters based on the input population. It is not possible at this stage to infer that Lenke Type-1 should be divided in 5 groups. However, this study confirms that within a defined 2D class currently used for surgical planning, there exists a number of sub-groups with different 3D signatures that are statistically significant. Therefore, each sub-group would lead to different surgical strategies. Previous studies have indicated that within Lenke Type-1 [5, 7, 15], there indeed exists 3D variability in terms of geometric parameters that could be divided in 4–6 sub-groups.

4 Conclusion

In this paper, we presented an automated classification method using a deep learning technique, namely with stacked auto-encoders, to discover sub-groups within a cohort of thoracic deformations. The code layer of the auto-encoder learns a distributed representation in low-dimension that aims to capture the main factors of variation in the training dataset. However, different examples from the distribution of the training dataset may potentially yield to high reconstruction errors [2]. Therefore, having a large and representative training dataset of AIS is critical. This will also prevent the model from overfitting.

The current study evaluated the 3D sub-classification of Lenke Type-1 scoliotic curves, suggesting that shape variability is present within an existing 2D group used in clinical practice. However, these types of approaches include complex synthesis tasks, which require sizeable datasets to improve the data representation within the code layer. Therefore, a multicentric dataset may help to significantly increase the number of cases from various sites and obtain a more reproducible model.

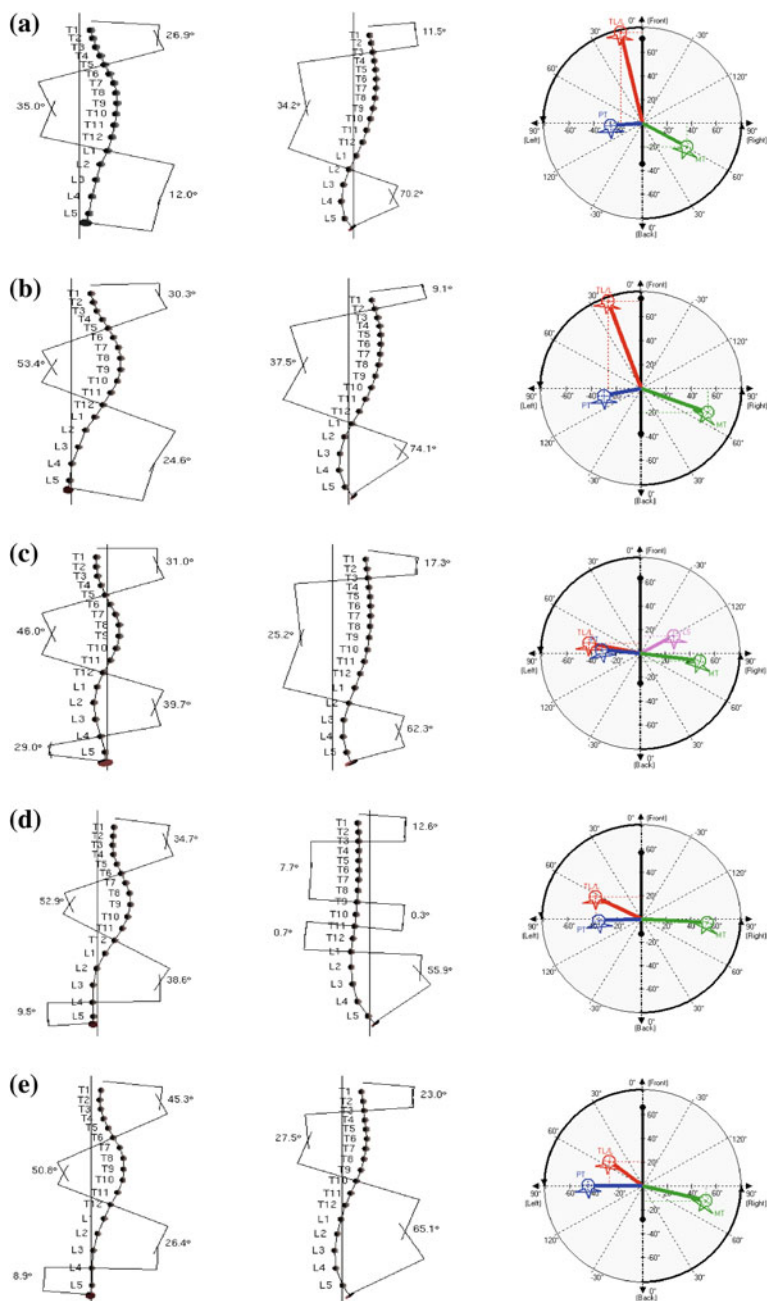


Fig. 5 Frontal, lateral and top view profiles of cluster centers, with da Vinci representations depicting planes of maximal deformities. **a** Centroid of cluster 1. **b** Centroid of cluster 2. **c** Centroid of cluster 3. **d** Centroid of cluster 4. **e** Centroid of cluster 5

Furthermore, the development of computational methods will ultimately lead to more reliable classification paradigms, helping to identify possible cases which might progress with time. Future work will include additional Lenke types, such as double major and lumbar deformations. Other works will propose to use longitudinal data for surgical treatment planning, whereas each observation is considered independently in the current framework. Finally, a reliability study will be undertaken to evaluate the relevance of classification systems.

References

1. Arthur, D., Vassilvitskii, S.: k-means++: The advantages of careful seeding. In: Proceedings of the eighteenth annual ACM-SIAM symposium on discrete algorithms. pp. 1027–1035. Society for industrial and applied mathematics (2007)
2. Bengio, Y., Courville, A., Vincent, P.: Representation learning: A review and new perspectives. *IEEE transactions on pattern analysis and machine intelligence* (2013)
3. Bergstra, J., Breuleux, O., Bastien, F., Lamblin, P., Pascanu, R., Desjardins, G., Turian, J., Warde-Farley, D., Bengio, Y.: Theano: a CPU and GPU math expression compiler. In: Proceedings of the Python for scientific computing conference (SciPy) (2010)
4. Duong, L., Cheriet, F., Labelle, H.: Three-dimensional classification of spinal deformities using fuzzy clustering. *Spine* **31**(8), 923–930 (2006)
5. Duong, L., Cheriet, F., Labelle, H.: Three-dimensional subclassification of lenke type 1 scoliotic curves. *J. Spinal Disord. and Tech.* **22**(2), 135–143 (2009)
6. Hinton, G., Salakhutdinov, R.: Reducing the dimensionality of data with neural networks. *Science (New York)* **313**(5786), 504–507 (2006)
7. Kadoury, S., Labelle, H.: Classification of three-dimensional thoracic deformities in adolescent idiopathic scoliosis from a multivariate analysis. *Euro. Spine J.* **21**(1), 40–49 (2012)
8. King, H.A., Moe, J.H., Bradford, D.S., Winter, R.B.: The selection of fusion levels in thoracic idiopathic scoliosis. *J. Bone and Jt. Surg.* **65**(9), 1302–1313 (1983)
9. Labelle, H., Aubin, C.E., Jackson, R., Lenke, L., Newton, P., Parent, S.: Seeing the spine in 3d: how will it change what we do? *J. Pediatr. Orthop.* **31**, S37–S45 (2011)
10. Lenke, L., Betz, R., Harms, J., Bridwell, K., Clements, D., Lowe, T., Blanke, K.: Adolescent idiopathic scoliosis: a new classification to determine extent of spinal arthrodesis. *J. Bone Jt. Surg. Am. bf 83-A*(8), 1169–1181 (2001)
11. van der Maaten, L.J., Postma, E.O., van den Herik, H.J.: Dimensionality reduction: A comparative review. *J. Mach. Learn. Res.* **10**(1–41), 66–71 (2009)
12. Pedregosa, F., Varoquaux, G., Gramfort, A., Michel, V., Thirion, B., Grisel, O., Blondel, M., Prettenhofer, P., Weiss, R., Dubourg, V., Vanderplas, J., Passos, A., Cournapeau, D., Brucher, M., Perrot, M., Duchesnay, E.: Scikit-learn: Machine learning in Python. *J. Mach. Learn. Res.* **12**, 2825–2830 (2011)
13. Pomero, V., Mitton, D., Laporte, S., de Guise, J.A., Skalli, W.: Fast accurate stereoradiographic 3d-reconstruction of the spine using a combined geometric and statistic model. *Clin. Biomech.* **19**(3), 240–247 (2004)
14. Ray, S., Turi, R.H.: Determination of number of clusters in k-means clustering and application in colour image segmentation. In: Proceedings of the 4th international conference on advances in pattern recognition and digital techniques. pp. 137–143 (1999)
15. Sangole, A.P., Aubin, C., Labelle, H., Stokes, I.A.F., Lenke, L.G., Jackson, R., Newton, P.: Three-dimensional classification of thoracic scoliotic curves. *Spine* **34**(1), 91–99 (2009)
16. Stokes, I.A., Bigalow, L.C., Moreland, M.S.: Measurement of axial rotation of vertebrae in scoliosis. *Spine* **11**(3), 213–218 (1986)

17. Stokes, I.A., Sangole, A.P., Aubin, C.E.: Classification of scoliosis deformity 3-d spinal shape by cluster analysis. *Spine* **34**(6), 584–590 (2009)
18. Vincent, P., Larochelle, H., Bengio, Y., Manzagol, P.A.: Extracting and composing robust features with denoising autoencoders. In: *Proceedings of the 25th international conference on machine learning*. pp. 1096–1103. ACM (2008)

Recent Advances in Computational Methods and
Clinical Applications for Spine Imaging

Yao, J.; Glocker, B.; Klinder, T.; Li, S. (Eds.)

2015, XVII, 259 p. 100 illus., Hardcover

ISBN: 978-3-319-14147-3